

Magnetic Circuit Model for the Mutually Coupled Switched-Reluctance Machine

James M. Kokernak and David A. Torrey, *Member, IEEE*

Abstract—The mutually coupled switched-reluctance motor (SRM) appears to have several performance advantages over other motor technologies. The existence of strong coupling between phases, however, makes the analysis of this machine quite complicated. Preliminary design of this machine can be greatly accelerated by the ability to evaluate potential motor geometries quickly. This paper introduces a general magnetic circuit model of the mutually coupled SRM that adapts to any geometry, unlike existing geometry-dependent approaches (such as finite elements), which are numerically intensive and require excessive computation time. The model uniquely implements the magneto-motive force (mmf) sources necessary to accommodate complex flux paths through the machine and includes the effects of magnetic saturation. The results are compared to those of a finite element solver to demonstrate the performance of this method as a first-step to evaluating candidate designs.

I. INTRODUCTION

RECENT advances in power electronic technology have made the switched-reluctance machine (SRM) an attractive choice for many applications. The conventional SRM has phase windings concentrated around individual stator poles and is shown in Fig. 1. In [1] and [2], an SRM is introduced that employs full-pitched windings on the stator, as shown in Fig. 2. Introducing magnetic coupling between phases can improve the switching characteristics of the converter and increase the average torque output of the machine [1]–[4]. The fully coupled machine is, however, far more difficult to model. A fast model for this machine, capable of providing a general evaluation of potential motor designs, is a powerful tool that can save the designer a great deal of time and computational resources. The advantage is the ability to discard inferior motor designs quickly and concentrate detailed design work on more promising designs. This method is not meant to replace finite element or other accurate numerical solutions. The model presented in this paper does not require time-consuming data entry and meshing. The results presented in this paper can be obtained in a matter of minutes.

While the SRM is simple in principle, it is rather difficult to design and develop performance predictions. This is due to the nonlinear magnetic characteristics of the machine under normally saturated operation. In [5], a modeling process is outlined for the conventional SRM. Due to the winding arrangement in

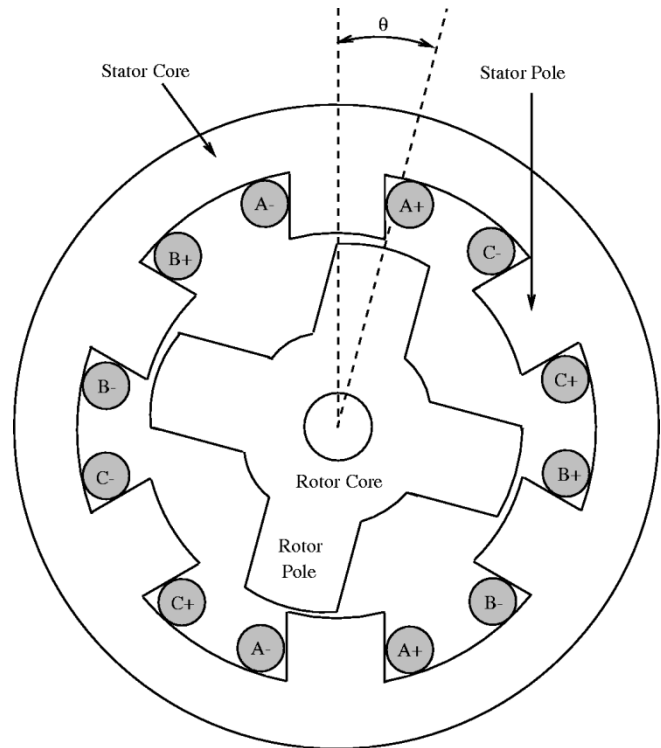


Fig. 1. The conventional SRM with windings concentrated around individual poles.

the conventional SRM, mutual coupling between phases is generally neglected. Phase flux linkage depends only on the rotor position and the current in the phase of interest; the phases are taken to be magnetically independent. Conversely, the mutually coupled SRM phases are magnetically coupled and the flux linking any particular phase is a function of rotor position and the currents in all phases.

While the mutually coupled SRM seems to promise a substantial advantage over the conventional SRM [1], [2] and other motor technologies, its performance remains relatively uncharacterized. The difficulty in modeling the mutually coupled SRM results from the phase-to-phase interaction and the nonlinear permeability of the steel. Superposition of two or more conventional SRM models to represent the mutually coupled machine is valid if the steel is considered to have constant permeability. If nonlinear characteristics are used, then saturation in the back iron is likely and superposition becomes invalid.

This paper presents a magnetic circuit model for the SRM with full-pitched windings. The model determines the flux linkage of each phase for any geometry, phase count, rotor position, and combination of phase currents. The model has

Manuscript received April 20, 1999; revised November 3, 1999. This work was supported in part by the Niagara Mohawk Power Electronics Research Chair and the New York State Energy Research and Development Authority. This paper is based on the Ph.D. dissertation of the first author.

The authors are with the Department of Electric Power Engineering, Rensselaer Polytechnic Institute, Troy, NY 12180-3590 USA.

Publisher Item Identifier S 0018-9464(00)01838-0.

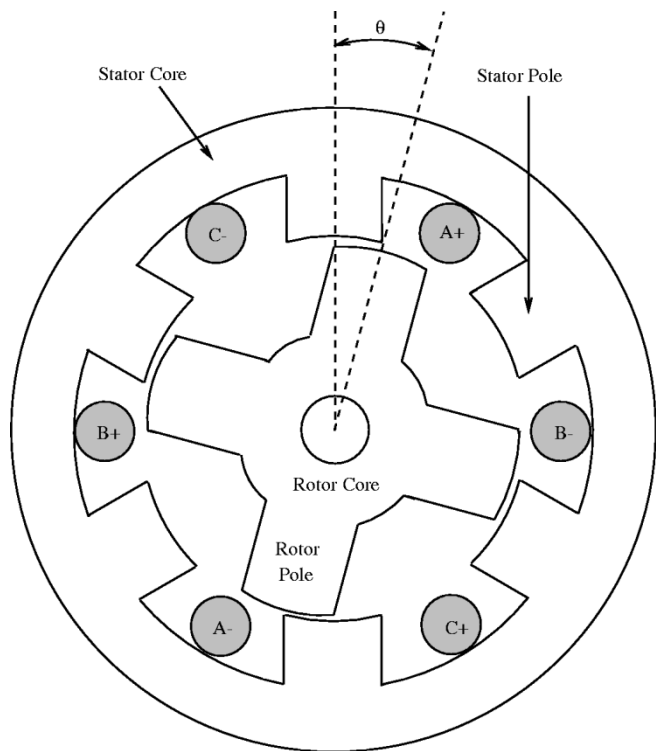


Fig. 2. The mutually coupled SRM with full-pitched windings.

been implemented in the C++ programming language. A magnetic circuit model that accurately determines machine flux for any combination of phase currents and rotor position sets the stage for a complete design package for the mutually coupled SRM. The results of this model are verified against the Flux2D finite element solver [7].

II. THE MAGNETIC CIRCUIT MODEL

This section outlines the development of a magnetic circuit model that allows the rotor and stator geometries of any specific mutually coupled SRM to be incorporated into a generic structure. This allows the solution process to work with any selected geometry. The magnetic circuit itself is analogous to an electric circuit except that admittances are replaced by permeances, voltages are replaced by sources of magneto-motive force (mmf), and currents are replaced by flux. The magnetic circuit approach is a powerful tool for electric machine design and has been presented in great detail [6].

The permeance circuit of the coupled machine is similar to that of the conventional SRM. This is because the general structures of the rotor and stator are similar for the conventional and mutually coupled machines. The major differences are due to dissimilar winding strategies. Each region of the machine is represented by a permeance that is a function of the geometry and permeability. For this model, separate permeances are used to represent the rotor poles, rotor back iron, stator poles, stator back iron, pole tips, and airgap permeances. Permeances associated with steel are assumed to be nonideal and are allowed to saturate. Airgap permeances are assumed to be ideal. The model parameters defined here are only geometry dependent, so the user should be able to automate the simulation to operate with

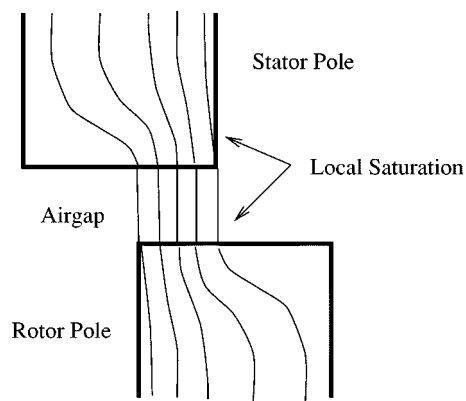


Fig. 3. Local saturation of pole tips when partially overlapped.

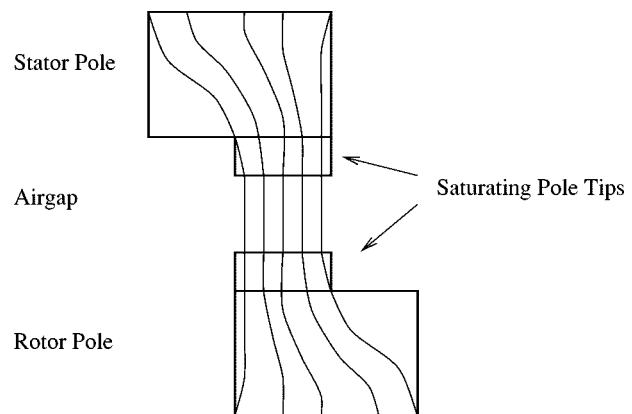


Fig. 4. Pole tip permeance dependent on rotor position and mmf drop.

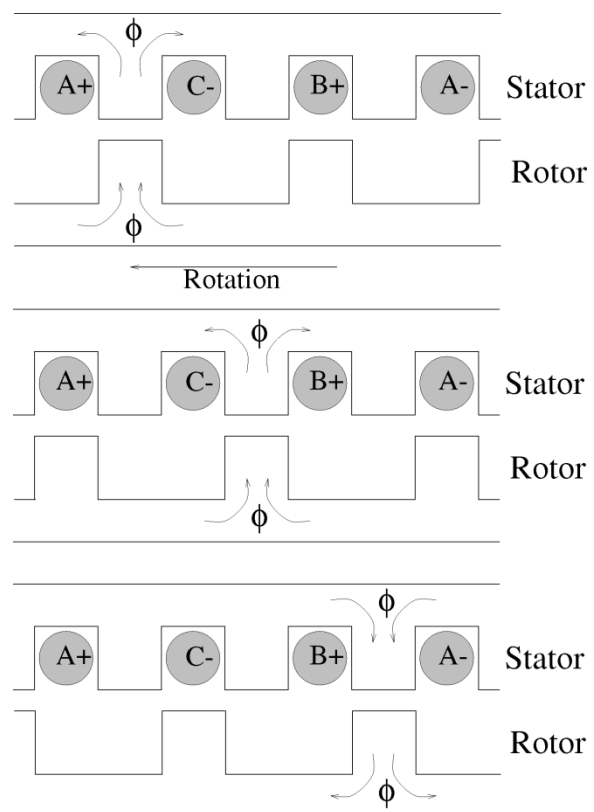


Fig. 5. Flux linking phase A due to current in phase B for three different rotor positions. Notice that flux linkage changes polarity with rotor position.

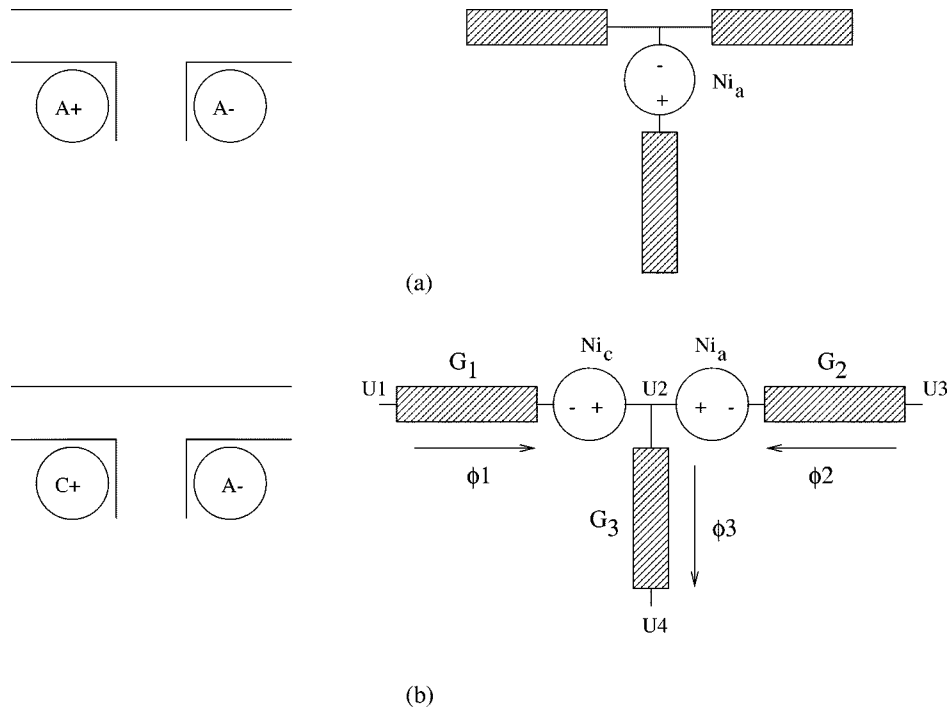


Fig. 6. Placement of mmf sources for (a) conventional and (b) mutually coupled SRM's.

only information on the number of poles, critical machine radii, pole angles, and machine length. These dimensions must be provided by the user.

The rotor and stator pole permeances must be handled carefully. When a rotor and stator pole exhibit partial overlap, the flux through each pole must pass through a smaller cross-sectional area at the airgap. While this flux may be insufficient to saturate the pole trunks, its flux density will increase at the airgap near the region of overlap. As a result, the poles of the machine will exhibit nonuniform flux densities. This causes a problem in the magnetic circuit model when local saturation occurs in the pole tips. Fig. 3 demonstrates this condition.

To deal with partial overlap, the stator and rotor poles can be divided into multiple permeances. The pole trunks can be represented as before but a "saturable pole tip" is included that varies its cross-sectional area with the region of overlap. This allows the flux path to be constricted in the airgap region, capturing the attendant local saturation. The inclusion of these pole tips is shown in Fig. 4. The relative dimensions of these pole tips depend on the flux density the machine will experience and the depth of saturation in the pole. Simulations have shown that predictions have reasonable accuracy if the pole tips are 10%–20% of the pole height.

An unfortunate consequence of adding the pole tips is the increase in both the number of permeances and nodes in the magnetic circuit. These factors contribute to increased simulation times. For this model, the single pole tip permeances for the rotor and stator poles were combined into a single permeance and included on the stator poles. This is acceptable since it effectively combines two series permeances. The motivation behind incorporating the permeances in this manner is minimizing the number of system nodes. It should be noted that increasing

the number of permeances comprising the poles increases accuracy at the expense of computation time.

A. MMF Source Placement

A major difference between the mutually coupled SRM and the conventional SRM models is how the mmf sources must be incorporated. In a conventional SRM, the phase windings direct flux through specific stator poles, so the mmf sources can simply be included in series with the stator pole permeances. The mutually coupled SRM sees flux directed ambiguously through the rotor, so mmf placement is not so clear. Fig. 5 demonstrates how the flux produced by one phase can link other phases in a positive or negative manner and is not restricted to a single stator pole.

An appropriate way to include the mmf sources is to assume that no flux escapes the stator back iron. The premise that all flux lines must close upon themselves dictates that whatever flux links a particular coil must pass through the stator back iron just behind that coil. This results in breaking each coil into two mmf sources associated with the winding slots of a particular phase. Each one has a value of Ni and is positioned in the stator back iron behind the winding, not in the stator pole. Fig. 6 shows how this differs from the conventional SRM model. The completed circuit model proposed here is shown in Fig. 7.

III. AIRGAP PERMEANCES

There are four different permeances which are included in the airgap model: overlap; fringing; slot leakage; and pole-to-pole leakage. They are all determined by flux tube analysis, although other approaches could be incorporated.

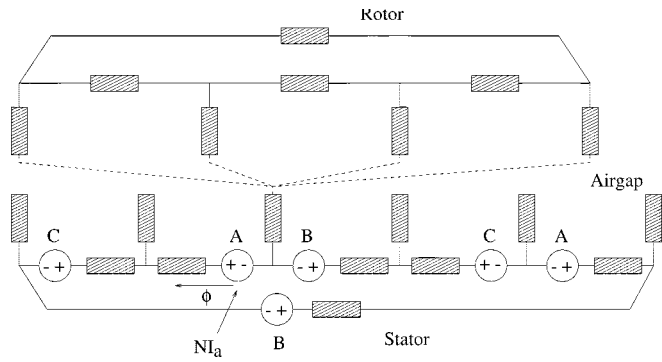


Fig. 7. The magnetic circuit model of the mutually coupled SRM. The shaded elements represent saturable portions of the machine. The dashed lines represent linear airgap permeances between one stator pole and all rotor poles. Similar reluctances would be included for each stator pole. The saturable pole tips are included in the pole permeances and are not represented separately in the figure.

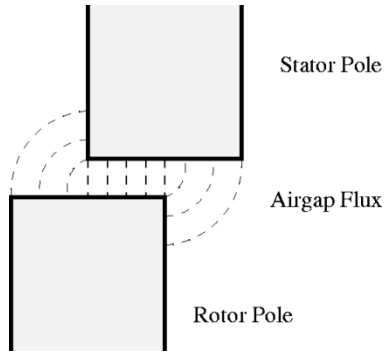


Fig. 8. Flux tubes representing airgap of partially overlapping poles.

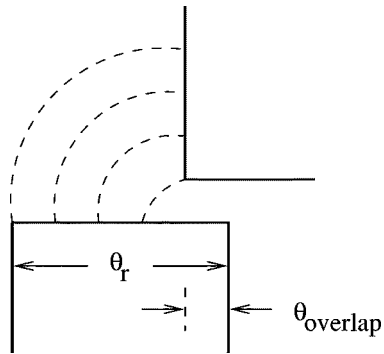


Fig. 9. Flux tube representing fringing effects at partially overlapping poles.

A. Overlap Permeances

The overlap permeance is that which occurs directly between rotor and stator poles in the region of overlap. The maximum possible permeance occurs when a rotor and stator pole pair are completely overlapped. This maximum permeance is given by

$$G_{\max} = \left(\frac{\mu_0 l \theta_{\max}}{g} \right) \left(\frac{r_{\text{sp}} + r_{\text{rp}}}{2} \right) \quad (1)$$

where l is the axial length of the machine, g is the radial airgap length, and θ_{\max} is the maximum possible overlap angle between the rotor and stator pole face. Radii r_{sp} and r_{rp} belong to the stator pole and rotor pole faces, respectively.

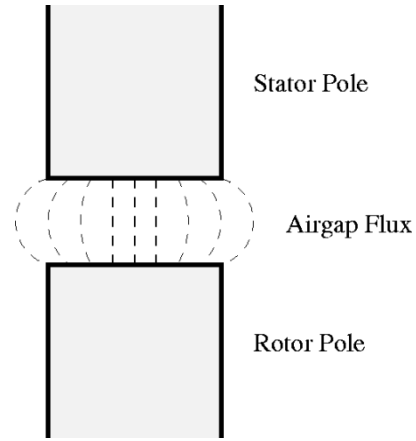


Fig. 10. Flux tubes representing airgap of completely overlapping poles.

The permeance between the i th stator pole and the j th rotor pole which exhibit some overlap, θ_{overlap} , is expressed by

$$G_{i,j} = \left(\frac{\theta_{\text{overlap}}}{\theta_{\max}} \right) G_{\max}. \quad (2)$$

The effects of fringing are considered separately.

B. Fringing Permeances

Fringing permeances occur in two instances. The first is when there is partial overlap between poles. In this case the fringing field is depicted as a bowing of flux lines from the face of one pole to the side of the overlapping pole. Fig. 8 demonstrates this case. The flux tube for this case can be approximated by a 90° wedge. The cross-sectional area of the wedge as shown in Fig. 9 is given by

$$A = l(\theta_r - \theta_{\text{overlap}})r_{\text{rp}} \quad (3)$$

where θ_r is the rotor pole pitch and l is the axial length of the machine. The average length of the flux tube is

$$L = \frac{(\theta_r - \theta_{\text{overlap}})r_{\text{rp}} \pi}{2}. \quad (4)$$

Combining (3) and (4) results in a partial overlap fringing permeance of

$$G_{\text{partial}} = \frac{\mu_0 A}{L} = \frac{4\mu_0 l}{\pi}. \quad (5)$$

The other case of fringing flux occurs when rotor and stator poles exhibit complete overlap as shown in Fig. 10. In this case, the flux tube is now a 180° semicircle (assuming the rotor and stator poles have the same width). Realizing that the flux tube is similar to that of the partial overlap case with twice the flux path length, it can be concluded that the permeance of the fully overlapped fringing is

$$G_{\text{full}} = \frac{2\mu_0 l}{\pi}. \quad (6)$$

C. Slot Leakage

The winding slot must be given extra attention since it is a current carrying region. The slot leakage path can be modeled with a series of concentric arcs as shown in Fig. 11. The current

in the slot is taken to be uniformly distributed so the current density in this region is taken to be

$$J = \frac{2Ni}{\theta_{\text{slot}} (r_{\text{sbi}}^2 - r_{\text{sp}}^2)}. \quad (7)$$

Assuming that the permeance of the steel is high compared to that of the slot, the magnetic field intensity between the poles at any given radius r is

$$H = \frac{Ni}{\theta_{\text{slot}} r} \frac{(r_{\text{sbi}}^2 - r^2)}{(r_{\text{sbi}}^2 - r_{\text{sp}}^2)}. \quad (8)$$

From this the flux between adjacent stator poles can be determined as a function of the radius

$$\phi = \frac{l\mu_0 Ni}{\theta_{\text{slot}} r} \frac{(r_{\text{sbi}} - r)(r_{\text{sbi}}^2 - r^2)}{(r_{\text{sbi}}^2 - r_{\text{sp}}^2)}. \quad (9)$$

The permeance of the slot is the total flux through the slot divided by the mmf drop across it. The total flux between stator poles is determined by evaluating (9) at $r = r_{\text{sp}}$. This results in

$$G_{\text{slot}} = \frac{\phi}{Ni} = \frac{\mu_0 l}{r_{\text{sp}} \theta_{\text{slot}}} (r_{\text{sbi}} - r_{\text{sp}}). \quad (10)$$

Again, l is the axial length of the machine.

D. Pole-to-Pole Leakage

Pole-to-pole leakage occurs when two nonoverlapping poles are close enough that flux passes from one to another. While this flux ideally is negligible, it plays an important role in determining machine fluxes in the unaligned and partially aligned positions. Fig. 12 shows the situation being considered and outlines the appropriate flux tubes to approximate the path. The flux path can be treated as a combination of those seen for the fringing and slot fluxes. The appropriate regions are numbered 1–4 in Fig. 12. Regions 1 and 2 are approximated as 90° arcs in the same manner as partial overlap fringing. Region 3 is a fraction of the current carrying slot and can be approximated by scaling (10) by the ratio $\theta_{\text{slot}}/\theta_{\text{space}}$. Region 4 is a series of concentric arcs in a source-free region. It is represented as

$$G_4 = \frac{\mu_0 (r_{\text{sp}} - r_{\text{rbi}}) l}{(r_{\text{sp}} - r_{\text{rbi}}) \theta_{\text{space}}} = \frac{2\mu_0 l}{\theta_{\text{space}}}. \quad (11)$$

Regions 1 and 4 and regions 2 and 3 are combined into two series branches. These two permeances form a parallel branch and are combined to one permeance from the rotor pole face to the stator pole face. Because the flux present in these regions is quite small, the simple flux tube provides reasonable results without impairing computational speed.

E. Complete Airgap

Once all of the various airgap permeances have been determined for a given rotor position, they must be incorporated into the model. Fringing and overlap permeances are combined together and included directly between the rotor and stator poles with which they are associated. Slot leakage permeances bridge the nodes of each stator pole face. A complete section of the

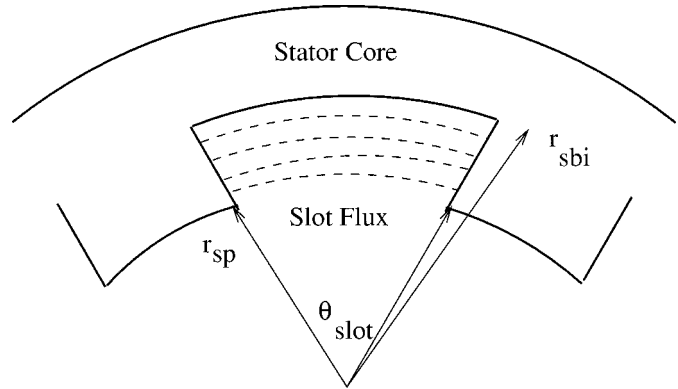


Fig. 11. Flux tubes representing flux paths in winding slots.

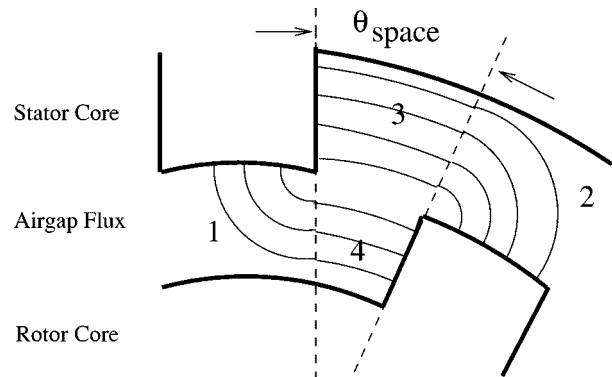


Fig. 12. Flux tubes representing flux paths between nonoverlapping poles.

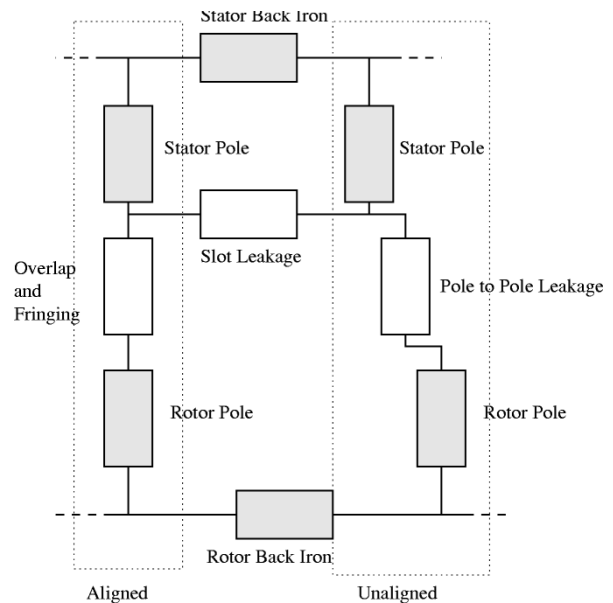


Fig. 13. A section of the magnetic circuit model including all types of permeances found in the airgap.

machine is shown in Fig. 13, which includes all airgap components.

IV. NONLINEAR SOLUTION

For the mutually coupled SRM with N_r rotor poles and N_s stator poles using one saturable pole tip element per stator pole, the magnetic circuit has $2(N_s + N_r) + N_s$ nonlinear elements.

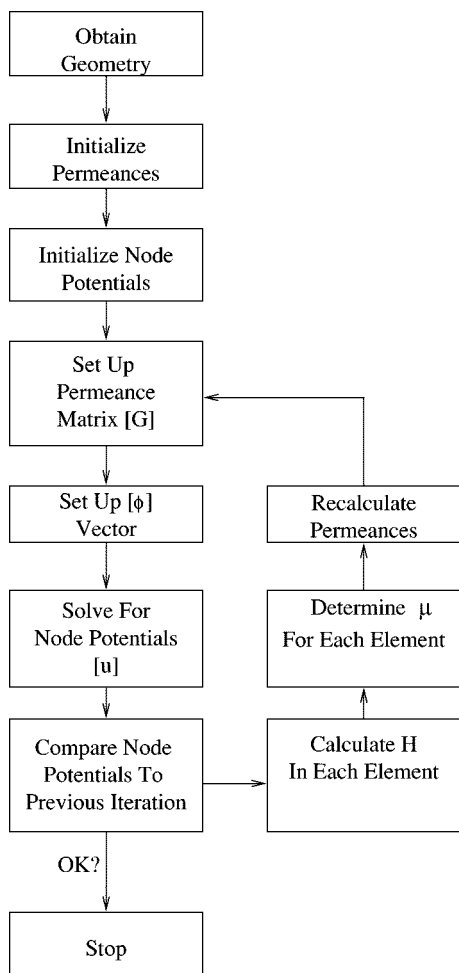


Fig. 14. Block diagram of the nonlinear solution procedure.

The number of linear airgap permeances is dependent on the relative rotor and stator pole sizes as well as the rotor pole angle. One solution approach would be to solve for the flux in each element, but the number of elements in the circuit could change with rotor position. A better approach is to solve for the magnetic scalar potential at every node in the circuit. This is analogous to solving for node potentials in an electric circuit as opposed to solving for mesh currents. Once the potentials at each node are determined, the flux through each branch can be determined from the mmf drop across the element. The total number of nodes in the system is constant regardless of rotor position and is dependent only on the number of poles in the machine.

The solution is set up by summing the flux at every node. Consider the section of the model as shown in Fig. 6(b). This portion of the machine is a stator pole with two sections of stator back iron and their associated sources of mmf. Using u to represent the magnetic scalar potential at the selected nodes, the equation at node 2 becomes

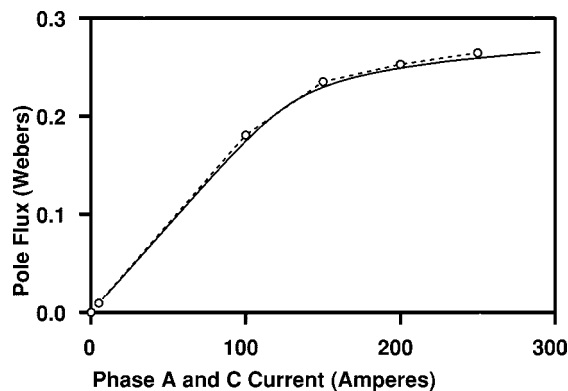
$$(u_1 + Ni_c - u_2)G_1 + (u_3 + Ni_a - u_2)G_2 = (u_2 - u_4)G_3. \quad (12)$$

This can be rearranged to become

$$u_2(G_3 + G_2 + G_1) - u_1G_1 - u_3G_2 - u_4G_3 = G_1Ni_c + G_2Ni_a. \quad (13)$$

TABLE I
DIMENSIONS OF SIMULATED
MACHINE

Radius to Housing (m)	0.450
Radius to Stator Back Iron (m)	0.350
Radius to Stator Pole Face (m)	0.300
Radius to Rotor Pole Face (m)	0.299
Radius to Rotor Back Iron (m)	0.249
Radius of Shaft (m)	0.159
Length of Machine (m)	1.00
Stator Pole Arc (degrees)	30
Rotor Pole Arc (degrees)	30
Number of Turns	10

Fig. 15. Stator pole flux as a function of phase currents at a rotor position of 0° . Flux2D results are represented by dashed line.

The complete set of node equations is a system which can be represented in matrix form

$$[G][u] = [\phi] \quad (14)$$

where $[G]$ is the $n \times n$ matrix of permeances, $[u]$ is the $n \times 1$ vector of node potentials, and $[\phi]$ is the $n \times 1$ vector of known fluxes. In all cases, n is dictated by the number of nodes in the system. This number does not change with rotor position, but it may be different for different geometries and pole configurations.

While the system matrix $[G]$ has an inverse, the individual permeances that make up the matrix are predominantly dependent on the node potentials and change as sections of the machine begin to saturate. For this reason an iterative procedure is required that updates the components of the system matrix at each iteration. For this simulation, a Gauss-Seidel solver was implemented. A block diagram of the solution procedure is shown in Fig. 14.

V. SIMULATION RESULTS

A simulation was performed for a mutually coupled SRM with six stator poles and four rotor poles. The dimensions of the machine are given in Table I. The flux was determined in the stator pole between phases A and C for several rotor positions while phases A and C were excited. Verification of the results was obtained with the Flux2D finite element package at several points. Fig. 15 shows the flux versus current curve in the aligned position. Figs. 16–18 show similar curves for rotor positions at

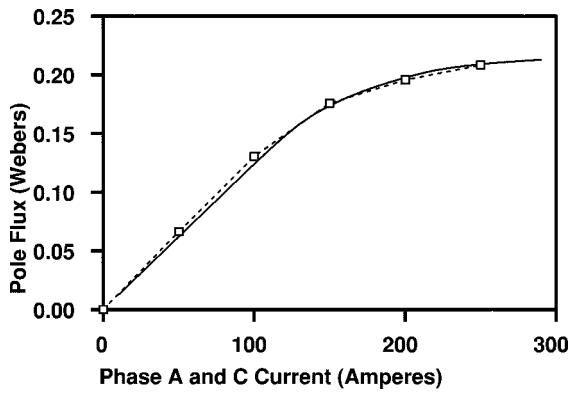


Fig. 16. Stator pole flux as a function of phase currents at a rotor position of 10° . Flux2D results are represented by dashed line.

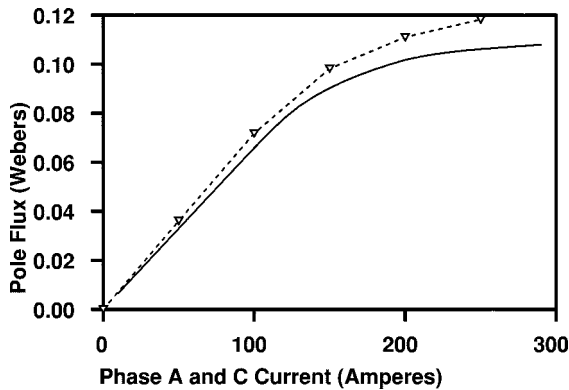


Fig. 17. Stator pole flux as a function of phase currents at a rotor position of 20° . Flux2D results are represented by dashed line.

10° , 20° , and 30° (completely unaligned position), respectively. Rotor positions are given in mechanical degrees.

Fig. 19 puts these curves on the same scale to show their relative variation. The error is small for the aligned position but increases somewhat as the rotor moves out of alignment. This discrepancy can be attributed to the small number of elements in the model, particularly in the poles, and the greater emphasis on airgap elements as flux is forced through the center pole. To verify this, a simulation was performed where the stator poles were implemented with an additional stator pole tip to further subdivide the pole. Fig. 20 demonstrates the improvement in representing the stator poles with three nonlinear elements as opposed to two.

The discrepancy seen in Fig. 18 should have a small effect on any performance prediction. This is concluded because the area between the upper and lower curves of Fig. 19 represents the amount of energy available for conversion by the machine. The slight variation in the lower curve has a small effect on that area. Fig. 21 shows stator pole flux as a function of rotor position for two phase currents. The top trace of 250-A forces the machine into saturation while the lower trace at 100 A does not.

VI. CONCLUSION

The authors of [8] and [9] present models for the conventional SRM that include mutual coupling, however, a fast and accurate model of the SRM with this winding strategy does not presently appear to exist. While this new machine exhibits a potential per-

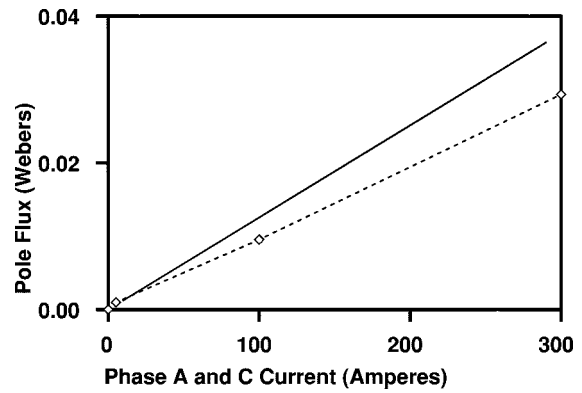


Fig. 18. Stator pole flux as a function of phase currents at a rotor position of 30° . Flux2D results are represented by dashed line.

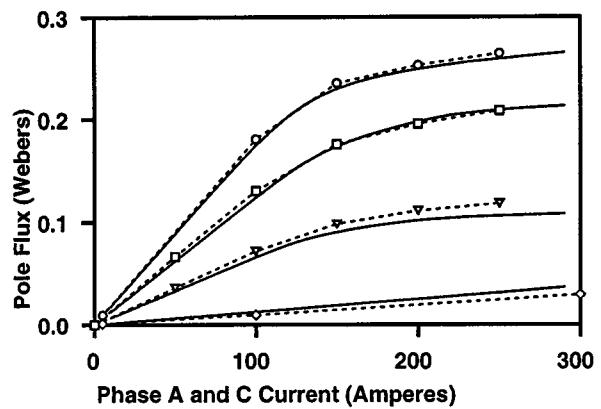


Fig. 19. Stator pole flux at various rotor positions as determined with the magnetic circuit model and Flux2D. The dashed lines represent the finite element solution. The data represented by the diamonds represent the unaligned position, triangles represent 20° , squares represent 10° , and circles represent the aligned position.

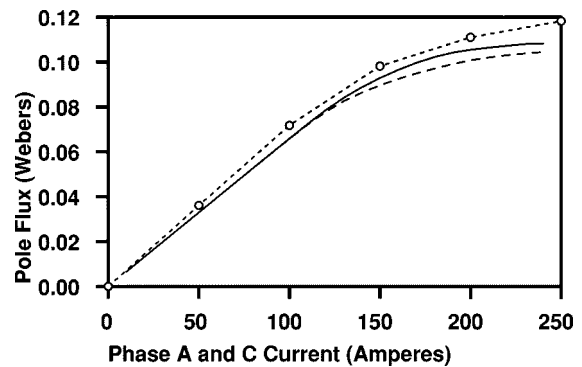


Fig. 20. Stator pole flux as a function of phase currents at 20° . The long-dashed line represents the original results with two nonlinear elements per stator pole. The solid line represents the results when three nonlinear elements are used. The dotted line with markers represents the Flux2D results.

formance advantage over existing technology, it cannot be seriously considered until its performance is well characterized. The first step to developing a working design model of this machine is to develop an accurate nonlinear magnetic model that can quickly evaluate candidate designs. This paper provides such a model.

A magnetic model has been presented that solves for machine fluxes based on phase currents. The flux values have been veri-

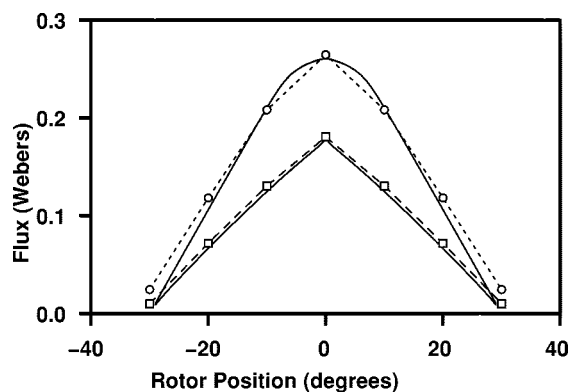


Fig. 21. Stator pole flux as a function of rotor position for phase currents of 250 A (top) and 100 A (bottom). Flux2D results are shown in dashed lines.

fied with a finite element package with very good accuracy and with a substantial speed advantage. Performance predictions for one electrical cycle could be obtained in less than 5 min with the magnetic circuit model. A single rotor position required ten minutes with the finite element solver. The node density of the mesh is a factor and must increase with small airgap machines. The stage has now been set to perform a detailed performance evaluation of the mutually coupled SRM to see if the performance improvements suggested in [1] and [2] relative to the conventional SRM can be realized. The model approach presented here is also suitable for conventional SRM geometries that require consideration of mutual coupling effects. Additional numerical algorithms can translate model flux solutions to motor torque predictions. Further efforts to generalize the saturable pole tip to various geometries are recommended, as well as investigation of the torque prediction capabilities.

REFERENCES

- [1] B. C. Mecrow, "New winding configurations for doubly salient electric machines," in *Proc. IEEE Industry Applications 27th Annu. Meeting*, 1992, pp. 249–256.
- [2] —, "Fully pitched-winding switched-reluctance and stepping-motor arrangements," *Proc. Inst. Elect. Eng.—B*, vol. 140, no. 1, pp. 61–70, Jan. 1993.
- [3] F. Liang, Y. Liao, and T. Lipo, "A new variable reluctance motor utilizing an auxiliary commutation winding," in *Proc. IEEE Industry Applications Society 27th Annu. Meeting*, 1992, pp. 219–225.

- [4] S. Li, F. Liang, Y. Zhao, and T. Lipo, "A doubly salient doubly excited variable reluctance motor," *IEEE Trans. Ind. Applicat.*, vol. 31, Jan./Feb. 1995.
- [5] D. A. Torrey and J. H. Lang, "Modeling a nonlinear variable-reluctance motor," *Proc. Inst. Elect. Eng.—B*, vol. 137, no. 5, pp. 314–326, Sept. 1990.
- [6] V. Ostovic, *Dynamics of Saturated Electric Machines*. New York: Springer-Verlag, 1989.
- [7] *Flux2D Finite Element Solver, v7.11*, MAGSOFT Corp., Troy, NY.
- [8] M. A. Preston and J. P. Lyons, "A switched reluctance motor model with mutual coupling and multi-phase excitation," *IEEE Trans. Magn.*, vol. 27, pp. 5423–5425, Nov. 1991.
- [9] J. C. Moreira and T. A. Lipo, "Simulation of a four phase switched reluctance motor including the effects of mutual coupling," *Electric Machines Power Syst.*, vol. 16, pp. 281–299, 1989.

James M. Kokernak received the B.S. degree in electrical engineering from Worcester Polytechnic Institute, Worcester, MA, in 1992 and the M.Eng. and Ph.D. degrees in electric power engineering from Rensselaer Polytechnic Institute, Troy, NY, in 1993 and 1997, respectively.

He joined the faculty at Rensselaer Polytechnic Institute as an Assistant Professor in July 1998. Since 1995, he has worked toward the development of efficient, high-performance switched-reluctance motor and generator drive systems. His recent industrial involvement includes the design, prototype, and development of a switched-reluctance direct-drive starter alternator for hybrid electric vehicle systems. His current research projects include the investigation of switched-reluctance technology for wind turbines, the development of new reluctance motor technology for adjustable speed drive applications, noise reduction in SRM's, and amorphous metals in electric machines. His research interests deal with high power quality, efficient energy conversion systems, and the problems associated with their implementation. Such systems include advanced electric machines, solar photovoltaics, microturbines, and fuel cells coupled to a power electronic interface for high-quality power delivery.

Dr. Kokernak is a member of ASEE, Sigma Xi, Tau Beta Pi, and Eta Kappa Nu. He is active within the IEEE Power Electronics Society.

David A. Torrey (S'80–M'81) received the B.S. degree in electrical engineering from Worcester Polytechnic Institute, Worcester, MA, and the S.M., E.E., and Ph.D. degrees in electrical engineering from Massachusetts Institute of Technology, Cambridge.

He spent three and a half years on the faculty at Worcester Polytechnic Institute before joining the faculty at Rensselaer Polytechnic Institute, Troy, NY, where he is the holder of the Niagara Mohawk Power Electronics Research Chair and an Assistant Professor in the Department of Electric Power Engineering. His research activities are focused on electric machine systems, with emphasis on switched-reluctance technology.

Dr. Torrey has been involved in IEEE activities that support power electronics through the Applied Power Electronics Conference. He is a registered professional engineer in New York State and a member of Sigma Xi, Tau Beta Pi, and Eta Kappa Nu.